JOURNAL OF COMPUTATIONAL PHYSICS 48, 423–440 (1982)

General Relaxation Schemes in Multigrid Algorithms for Higher-Order Singularity Methods

B. OSKAM AND J. M. J. FRAY

National Aerospace Laboratory, NLR,
1059 CM Amsterdam, The Netherlands

Received January 15, 1982

Relaxation schemes based on an approximate and incomplete factorization technique (AF) are described. These AF schemes allow one to construct a fast multigrid method for solving integral equations of the second as well as of the first kind. Novel items are the smoothing factors found for integral equations of the first kind and the comparison with similar results for equations of the second kind. Application of the MG algorithm shows convergence of a second-order accurate panel method to the level of the truncation error within two multigrid cycles.

INTRODUCTION

Most effort going into the application of multigrid techniques seems to be directed to solving the sparse systems of difference equations associated with partial differential equations. The multigrid technique, however, can also be used advantageously to solve the nonsparse systems of equations that arise from integral equations, as shown in [1, 2].

In the present paper we study the application of multigrid techniques to the solution of integral equations associated with potential flow problems. This effort fits into the larger framework of the development, at NLR, of a next generation singularity or "panel" method. A question associated with this development is whether singularity methods do have a future, particularly in view of the current progress in finite difference methods. Slooff [3] presents several arguments for a positive answer to this question, but at the same time presents the rather stringent requirement of high computational efficiency. The scope of the present investigation is limited to the analysis of multigrid (MG) techniques and the subsequent application to some model problems in two dimensions. Various relaxation schemes, which are used as smoothing operators in multigridding, are evaluated. For some particular geometries, such as an unbounded flat plate and a circular cylinder, this smoothing problem is analyzed by the local mode analysis of [4]. For more complicated geometries, such as an airfoil, it is found that the finite-dimensional discrete Fourier transform can be used to define a global smoothing factor which

0021-9991/82/120423-18$02.00/0
Copyright © 1982 by Academic Press, Inc.
All rights of reproduction in any form reserved.

581/48/3-8

represents an upper bound of the actual convergence factor of the high-frequency components of the residual vector. A general multigrid algorithm is described and applied to solve the potential flow problem of multicomponent airfoils.

Before starting the discussion of the integral equations it is important to realize that the asymptotic operation counts remain of the order of n^2 if nothing is done to reduce the work associated with the residue evaluations which involve a full matrix times vector multiplication. Multigrid methods to lower the computational work involved with these residue evaluations are currently being studied at NLR [3]. The basic concept is to lower the asymptotic operation counts by treating the far field connections on a sequence of coarser grids without compromizing the truncation error. These aspects of a next generation panel method are, however, outside the scope of this paper.

Integral Equations

Most panel methods use the boundary condition of zero normal velocity on the surface of the contour to derive an integral equation for a distribution of surface singularity, source or doublet, over the body surface. Let us denote the source and doublet strength by σ and μ, respectively, and let $\mathbf{x}_p$ and $\mathbf{x}_q$ be the positions of the points p and q. The normal velocity at the point p induced by distributions of these singularities may be represented as

$$v_n^s(\mathbf{x}_p) = \frac{1}{2\pi} \int \sigma(\mathbf{x}_q) \frac{\partial}{\partial n_p} (\ln |\mathbf{r}_{pq}|)\, ds_q, \tag{1}$$

and

$$v_n^d(\mathbf{x}_p) = \frac{1}{2\pi} \int \mu(\mathbf{x}_q) \frac{\partial}{\partial n_p} \frac{\partial}{\partial n_q} (\ln |\mathbf{r}_{pq}|)\, ds_q, \tag{2}$$

where $\mathbf{r}_{pq} = \mathbf{x}_p - \mathbf{x}_q$ and n_q is the outward normal, and direction of the doublet axis, at the point q. The normal at $\mathbf{x}_p$ is denoted by n_p. The integration variable s is the distance measured along the contour.

Attention is directed to two particular panel methods which may be formulated by employing Eqs. (1) and/or (2). The first is the surface source method having an unknown source distribution on the body surface and an auxiliary doublet distribution of known shape but unknown magnitude, also on the body surface, to produce the lift, see [5]. The second panel method considered employs Eq. (2) only and is called the doublet method, see, e.g., [6]. The reason these two methods have been employed in the present paper is that they produce quite different integral equations, being of the first and second kind for the doublet and source method, respectively.

To facilitate the discussion of various discretization schemes we rewrite Eq. (2) for the particular case of an unbounded flat plate as

$$v_n^d(x) = \frac{1}{2\pi}\int_{-\infty}^{+\infty} \frac{d^2\mu}{d\xi^2} \ln|x-\xi|\, d\xi - \frac{1}{2\pi}\int_{-\infty}^{+\infty} d\left(\frac{d\mu}{d\xi}\ln|x-\xi|\right) - \frac{1}{2\pi}\int_{-\infty}^{+\infty} d\left(\frac{\mu(\xi)}{x-\xi}\right), \tag{3}$$

where x, ξ is the distance measured along the plate.

Discretization of Integral Equations

The aerodynamic influence coefficients are evaluated using a consistent small curvature expansion of the integrals that remain after discretization [7]. Specifically, the profile curve that defines a two-dimensional body is approximated by a piecewise quadratic representation and the source and doublet distributions are approximated by piecewise linear and quadratic representations, respectively. These choices result in aerodynamic influence coefficients (AIC's) of second-order accuracy in h, where h is the panel size.

Let the doublet representation for the case of an unbounded flat plate be given by

$$\tilde{\mu}(\xi) = \mu_i + (d\mu/d\xi)_i(\xi-\xi_i) + (d^2\mu/d\xi^2)_i \tfrac{1}{2}(\xi-\xi_i)^2, \qquad |\xi-\xi_i| \leqslant h/2. \tag{4}$$

For the purpose of studying the dependency of the smoothing factor on the discretization scheme, the derivatives in Eq. (4) have been discretized by 3-point differences

$$(d\mu/d\xi)_i = (\mu_{i+1}-\mu_{i-1})/2h, \qquad (d^2\mu/d\xi^2)_i = (\mu_{i+1}-2\mu_i+\mu_{i-1})/h^2, \tag{5}$$

and by 5-point differences, resulting from a continuity requirement of $\tilde{\mu}$ across panel edges,

$$(d\mu/d\xi)_i = (-\mu_{i+2}+10\mu_{i+1}-10\mu_{i-1}+\mu_{i-2})/16h \tag{6a}$$

and

$$(d^2\mu/d\xi^2)_i = (-\mu_{i+2}+8\mu_{i+1}-14\mu_i+8\mu_{i-1}-\mu_{i-2})/4h^2, \tag{6b}$$

where μ_i is the value of the doublet representation $\tilde{\mu}$ at ξ_i, which is the midpoint of panel with index i. For the case of the flat plate all panels have equal size h. The difference between the 3-point and 5-point representations, $\tilde{\mu}_{3-p}$ and $\tilde{\mu}_{5-p}$, respectively, turns out to be

$$\tilde{\mu}_{5-p} - \tilde{\mu}_{3-p} = (h^2/8)(d^3\mu/d\xi^3)_i(\xi-\xi_i) + (h^2/8)(d^4\mu/d\xi^4)_i(\xi-\xi_i)^2, \tag{7}$$

which is of the same order in h as higher-order terms neglected in Eq. (4). Thus the 3- and 5-point differences both result in a doublet representation of third-order accuracy in h. Both representations have sufficient continuity at the panel edges such that the contributions of the second and third integral in Eq. (3) may be neglected, being not larger than the basic truncation error of the first integral in Eq. (3).

Evaluating Eq. (3) at panel control points, after substituting Eq. (4), results in a system of algebraic equations

$$v_n^d(x_i) = \frac{1}{2\pi h} \sum_{k=-\infty}^{+\infty} a_k \mu_{k+i}, \qquad i = -\infty, \ldots, \infty, \tag{8}$$

where

$$a_k = k \ln |1 + 32k/(2k-3)(2k+1)^3| + \tfrac{3}{2} \ln |1 - 8/(4k^2-1)|, \tag{9}$$

or

$$\begin{aligned} a_k = {} & \tfrac{9}{16} \ln |1 + 16/(4k^2-25)| + \tfrac{21}{8} \ln |1 - 8/(4k^2-1)| \\ & + \tfrac{1}{4} k \ln |1 - 8k/(4k^2+k-15)| \\ & + 2k \ln |1 + 8k/(4k^2-4k-3)| + \tfrac{7}{2} k \ln |1 - 2/(2k+1)|. \end{aligned} \tag{10}$$

Equation (9) represents the AIC's resulting from the 3-point differences in Eq. (5) and the AIC's of Eq. (10) correspond to 5-point differences (Eq. (6b)).

For the case of a curved contour such as an airfoil, we need a small curvature expansion of the integrals as mentioned before. Moreover, we shall take a nonuniform panel distribution. The resulting expressions of the AIC's will not be presented here for the sake of brevity. It should be mentioned, however, that the AIC's of the doublet distributions are based on a third-order accurate representation $\tilde{\mu}$, requiring continuity of $\tilde{\mu}$ across panel edges, which involves a generalization of the 5-point differences in Eq. (6) to nonuniform panels.

The resultant linear system of algebraic equations may be written as

$$\sum_{j=1}^{n+n_c} a_{ij} u_j = f_i, \qquad i = 1, 2, \ldots, n+n_c, \tag{11}$$

where n is the total number of surface panels and n_c the number of components of a multicomponent airfoil. The unknown parameters u_j for $j = 1, \ldots, n+n_c$ denote σ_j $(j = 1, 2, \ldots, n)$, c_j $(j = 1, \ldots, n_c)$, for the source method, where σ_j is the value of the source representation at control point $\mathbf{x}_j$ and c_j is the magnitude of the auxiliary doublet distributions of component j. In case of the doublet method u_j $(j = 1, 2, \ldots, n+n_c)$ denotes μ_j $(j = 1, 2, \ldots, n)$, μ_j^c $(j = 1, \ldots, n_c)$, where μ_j is the value of the doublet representation at control point $\mathbf{x}_j$ and μ_j^c the value of the doublet representation at the endpoint of the integration interval of component j. The value of the doublet distribution at the beginning of each integration interval is equated to

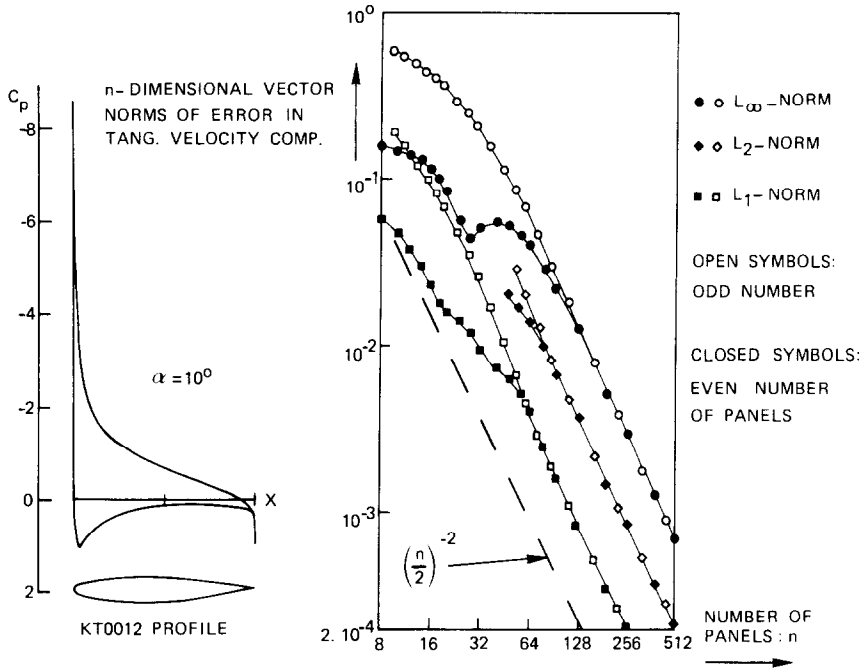

FIG. 1. Pressure distribution of 12-percent thick Kármán–Trefftz profile with 15° traling edge angle; discretization error of this solution as function of the number of panels.

zero without any loss of generality. The ordering of Eqs. (11) is such that the diagonal elements a_{ii} of the first n equations express the influence of a parameter u_i at the control point $\mathbf{x}_i$. The last n_c equations of system (11) express the Kutta conditions at the trailing edges of the airfoil components j ($j = 1,..., n_c$).

An example solution of the source method applied to a 12-percent thick von Kármán–Trefftz airfoil with a trailing edge angle of 15 degrees (KT0012) is shown in Fig. 1. Second-order convergence of the n-dimensional vector norms of the error in the velocity component of this solution is found, see Fig. 1.

RELAXATION SCHEMES

The relaxation schemes, also called smoothing operators in MG algorithms, exploit the behavior of the kernels of Eqs. (1) and (2), being like $1/r$ and $1/r^2$, respectively, where r denotes the distance. This behavior tells us that the high-frequency components of the singularity distribution have a short coupling range. Neglecting the far field connections between parameters and control points should, therefore, be a sound basis for constructing effective smoothing operators.

On the basis of this consideration we shall present two basic classes of relaxation schemes. The first class of shemes is based on incomplete LU factorization [8] of the approximate system of linear equations that remains after omitting the far field connections, resulting in an approximate factorization (AF). The factors L and U of the LU factorization are forced to have an extensive zero pattern by omitting the nonzero entries which may arise outside of the intended nonzero pattern in the factors L and U during factorization. The present AF scheme is different from the incomplete factorization of algebraic equations associated with the discretization of partial differential equations because there is no need to omit any far field connections in the latter. Moreover, the extensive zero pattern in the lower and upper triangular factors need not be the same as the zero pattern of the approximate system of linear equations that remains after omitting the far field connections, although we have chosen these two patterns identical in the present examples.

A second class of relaxation schemes is based on the direct construction of a sparse approximate inverse. We may construct such an inverse if we approximately satisfy each individual equation of system (11) in its turn by directly solving a very small system of equations, comprising a subset of the entries of the full system, for every unknown parameter. These small systems should be chosen such that they include the coupling range of high frequencies. Thus we relax each equation individually, distributing changes to its neighboring parameters. This second class, which we will call natural relaxation schemes (NRS), is also a general technique. An example of this technique is given in the next section.

Fourier Analysis

Let a relaxation scheme based on approximate factorization of Eq. (8) be defined by

$$\sum_{k=-n_a}^{n_a} a_k \mu_{k+i}^{(v+1)} = f_i - \sum_{k=-\infty}^{-n_a-1} a_k \mu_{k+i}^{(v)} - \sum_{k=n_a+1}^{\infty} a_k \mu_{k+i}^{(v)}, \tag{12}$$

where the superscript v is the iteration index and f_i the right-hand side which is given. The pattern of far field connections which are neglected in the approximate equation on the left-hand side of Eq. (12) is denoted by the integers k satisfying $|k| > n_a$. This zero pattern also applies to the factorization. The convergence factor ρ of the θ component, defined in [4], of the error in the solution during iteration procedure (12) is found to be

$$\rho(\theta) = \left| 2 \sum_{k=1+n_a}^{\infty} a_k \cos(k\theta) \right| \Big/ \left| a_0 + 2 \sum_{k=1}^{n_a} a_k \cos(k\theta) \right|, \tag{13}$$

where the second summation term is to be omitted for $n_a = 0$. This convergence factor as a function of the frequency θ is shown in Figs. 2 and 3 for $n_a = 0$, 1, 2, and

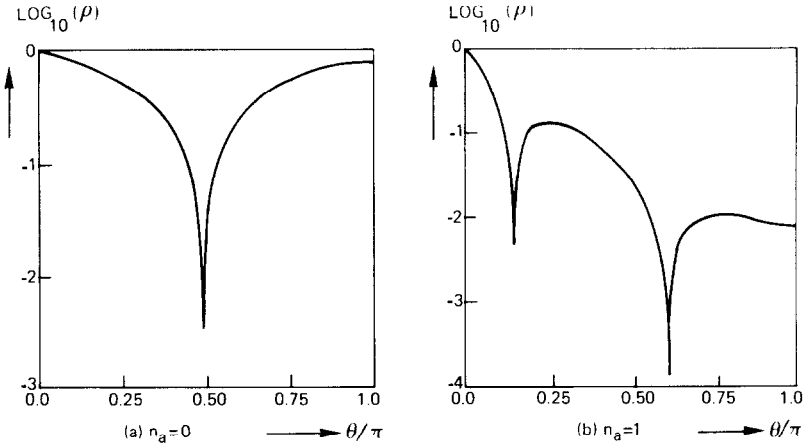

FIG. 2. Convergence factor as function of frequency for doublet method (Eq. (13) with 5-point differences); $n_a = 0$ and 1, AF scheme.

4. It is seen that the convergence of the high frequencies, i.e., $\theta > \pi/2$, is of the order of 10^{-2} for $n_a \geqslant 1$.

The second relaxation scheme (NRS) for Eq. (8) is based on a sparse inverse $\tilde{a}_k$ which is defined by

$$\begin{aligned} \tilde{a}_k &= 0, \qquad \text{for} \quad |k| > n_a, \\ &= g_k, \qquad \text{for} \quad |k| \leqslant n_a, \end{aligned} \tag{14}$$

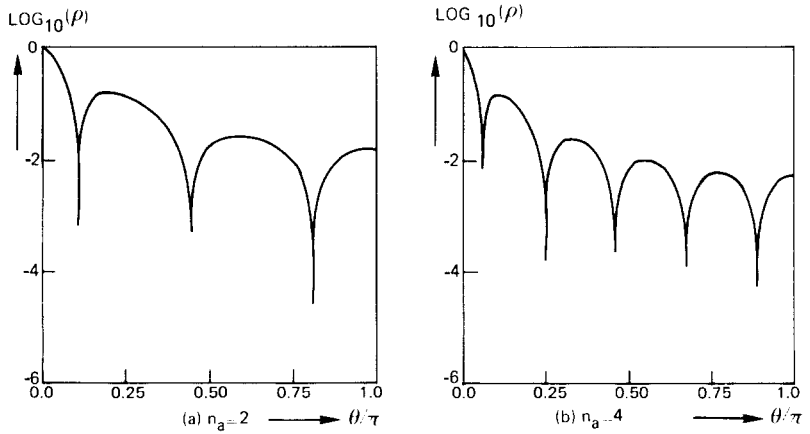

FIG. 3. Convergence factor as function of frequency for doublet method (Eq. (13) with 5-point differences); $n_a = 2$ and 4, AF scheme.

where g_k is the solution of

$$\sum_{j=-n_a}^{n_a} a_k g_j = \delta_{i0} \qquad \text{for} \quad i = -n_a, \ldots, n_a, \tag{15}$$

with $k = |j - i|$ and δ_{i0} = Kronecker delta. Applying this approximate inverse $\tilde{a}_k$ in a residual correction iteration process (see the Appendix) results in an error amplification matrix given by $I - \tilde{A}A$. The matrix $\tilde{A}A$, denoted by B, is an infinite symmetric Toeplitz matrix because A and $\tilde{A}$ are infinite symmetric Toeplitz matrices. This observation allows one to obtain the convergence factor implied by this NRS scheme, similarly to Eq. (13). One finds

$$\rho(\theta) = \left| 1 - b_0 - 2 \sum_{k=1}^{\infty} b_k \cos(k\theta) \right|, \tag{16}$$

where b_k are the elements of $B = A\tilde{A}$. It may be verified that Eqs. (13) and (16) are identical for $n_a = 0$. The local smoothing factor $\bar{\rho}$ is defined in [4] by

$$\bar{\rho} = \max_{\pi/2 \leqslant |\theta| \leqslant \pi} \{\rho(\theta)\}. \tag{17}$$

It is a significant measure by which the relative merits of Eqs. (13) and (16) may be judged for $n_a \geqslant 1$. Values of $\bar{\rho}$ for $n_a = 0$, 1, 2, 4, and 7 are given in Table I for both the 3- and 5-point difference schemes. It may be seen that the smoothing factor of the AF scheme is considerably better than that of the NRS scheme. Comparing the 3- and 5-point differences shows that in case of the AF scheme the 5-point differences result in a lower smoothing factor for $n_a \geqslant 1$.

TABLE I

Theoretical Smoothing Factors for Doublet Method with Normal-Velocity Boundary Conditions

	Unbounded flat plate				Circ. cylinder	
	3-point NRS Eq. (16)	5-point NRS Eq. (16)	3-point AF Eq. (13)	5-point AF Eq. (13)	5-point AF Eq. (18) $n = 512$	5-point AF Eq. (18) $n = 128$
$n_a = 0$	0.415	0.797	0.415	0.797	0.795	0.790
$n_a = 1$	0.406	0.543	0.163	0.0227	0.0232	0.0249
$n_a = 2$	0.321	0.421	0.0422	0.0251	0.0252	0.0255
$n_a = 4$	0.261	0.326	0.0156	0.0102	0.0102	0.0103
$n_a = 7$	0.202	0.256	0.0052	0.0037	0.0037	0.0037

Note. NRS, Natural relaxation scheme; AF, aprroximate factorization.

TABLE II

Theoretical Smoothing Factors for Source Method Applied to Circular Cylinder[a]

$n = 128$	$n = 256$	$n = 512$
0.00792	0.00397	0.00199

[a] Equation (18); $n_a = 0$.

Applying the source or doublet method to the parallel flow around a circular cylinder (no lift) results in a symmetric circulant matrix (Eq. (11)), which is denoted by c_k $(k = 0, 1, 2, \ldots, n-1)$, provided we use uniform paneling. The convergence factor of the errors in the solution during iteration procedure (12) applied to these circulants is found to be

$$\rho(\theta_i) = \left| c_{n/2} + 2 \sum_{k=1+n_a}^{n/2-1} c_k \cos(k\theta_i) \right| \Big/ \left| c_0 + 2 \sum_{k=1}^{n_a} c_k \cos(k\theta_i) \right|, \tag{18}$$

where the discrete frequencies θ_i extend over $2\pi i/n$, $i = 0, 1, \ldots, n/2$. Equation (18) turns out to be identical to Eq. (13) in the limit of $n \to \infty$. The smoothing factors obtained from Eq. (18) for the doublet method, as shown in Table I, reflect this observation. For the source method the smoothing factors obtained from Eq. (18) are given in Table II. These factors tend to zero in the limit of n going to infinity, which is characteristic for "MG algorithms of the second kind."

Although the results obtained above do give valuable insight into the smoothing properties of relaxation schemes, the local mode analysis cannot take the effects of such practical things as surface slope discontinuities and/or nonuniform paneling of the surface into account. An n-dimensional discrete Fourier transform of the residue amplification matrix $I - A\tilde{A}$ (see the Appendix) given by

$$G = F(I - A\tilde{A})F^{-1}, \tag{19a}$$

$$F = f_{kl} = \sqrt{1/n} \exp[i2\pi kl/n], \qquad k, l = 0, 1, \ldots, n-1, \tag{19b}$$

$$F^{-1} = F^* \text{ (the complex conjugate)}, \tag{19c}$$

is more suitable to study these aspects of the smoothing problem. The matrix $\tilde{A}$ in Eq. (19a) may either be an actual inverse (NRS) or the implied inverse of an AF scheme. Let the row sum of G be defined by

$$\lambda_k = \sum_{l=0}^{n-1} |G_{kl}|, \qquad k = 0, \ldots, n-1. \tag{20}$$

This row sum can be shown to be an upper bound of the convergence factor of the θ_k component of the residue vector in a residual correction iteration process, where

TABLE III

Global Smoothing Factors of Approximate Factorization (AF) for Source and Doublet Methods Applied to KT0012 Profile

	Source method				Doublet method (5-points)			
n	32	64	128	256	32	64	128	256
$n_a = 0$	1.35	1.36	1.35	1.34	1.75	1.83	1.87	1.89
$n_a = 1$	0.49	0.54	0.55	0.56	0.29	0.24	0.22	0.23
$n_a = 2$	0.32	0.36	0.34	0.34	0.24	0.23	0.22	0.22
$n_a = 4$	0.19	0.23	0.24	0.23	0.20	0.13	0.11	0.10

$\theta_k = 2\pi k/n$ occupies the unique part of the frequency range for $k = 0, 1, \ldots, n/2$. These considerations allow us to define a global smoothing factor $\bar{\lambda}$ by

$$\bar{\lambda} = \max_{n/4 \leqslant k \leqslant n/2} \{\lambda_k\}, \tag{21}$$

analogous to the local smoothing factor (Eq. (17)). It should be noted, however, that this global smoothing factor is only an upper bound of the convergence of the high-frequency components because the transformation in Eqs. (19b) and (19c) results in a matrix G which is not diagonal, the off-diagonal elements representing the coupling of differing frequencies.

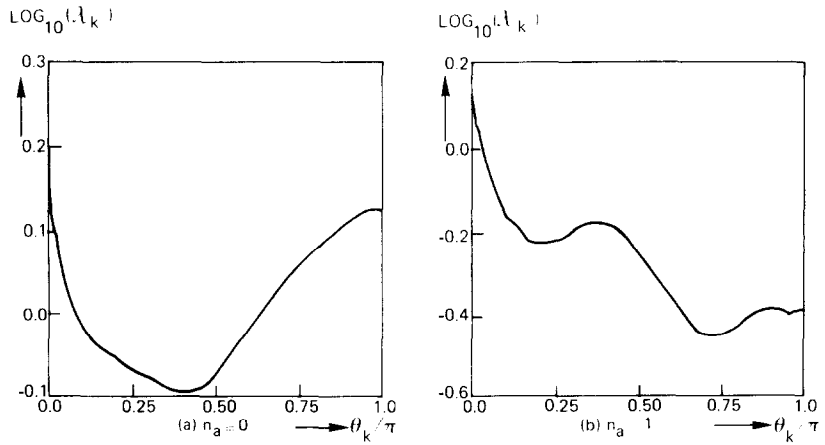

FIG. 4. Row sum of amplification matrix G as function of frequency for source method; KT0012, $n = 256$, $n_a = 0$ and 1, AF scheme.

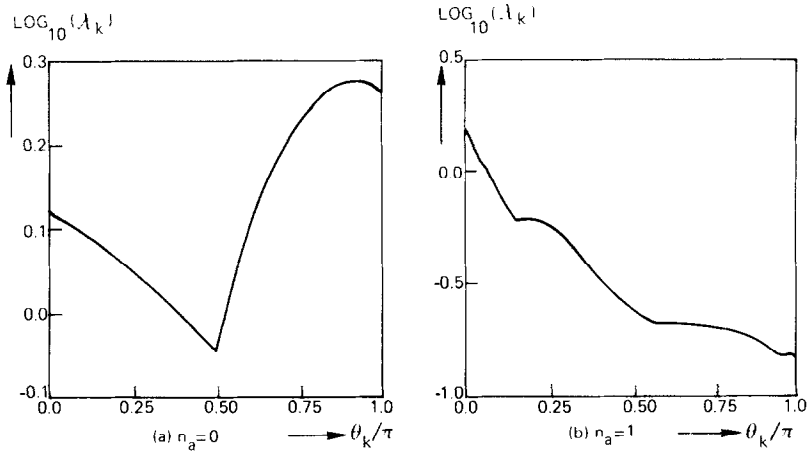

FIG. 5. Row sum of amplification matrix G as function of frequency for doublet method; KT0012, $n = 256$, $n_a = 0$ and 1, AF scheme.

The global smoothing factor of the AF scheme applied to the source and doublet method for the KT0012 profile (see Fig. 1) has been determined using a fast Fourier transform algorithm. The particular AF scheme used is characterized as before by the far field connections omitted from Eq. (11) and the subsequent zero pattern forced onto the incomplete LU factorization of the resultant sparse matrix. These two sets, the far field connections a_{ij} and the zero pattern, are defined by the pairs of integers (i, j) satisfying

$$|i-j| > n_a \qquad \text{and} \qquad |i+j-n-1| > n_a, \qquad i \leqslant n \qquad \text{and} \qquad j \leqslant n. \quad (22)$$

Table III gives the computed global smoothing factors for $n = 32$, 64, 128, and 256 and for $n_a = 0$, 1, 2, and 4. From this table the following conclusions are drawn: The smoothing improves as the dimension of the nonzero pattern n_a is increased. There is no qualitative difference between the source and doublet method, the smoothing factors being approximately independent of the number of panels. This is expected of the doublet method, but the source method results are qualitatively different from those of Table II. Numerical experiments suggest that this qualitative difference is a direct result of the surface slope discontinuity at the trailing edge.

The similarity between the source and doublet method may also be observed from the results plotted in Figs. 4 and 5, where the row sum λ_k is shown as a function of frequency for $n_a = 0$ and 1. When $n_a = 1$, a typical smoothing character is observed, i.e., the convergence bound λ_k decreases with increasing frequency.

MULTIGRID ALGORITHM

The multigrid algorithm is described by the following quasi-FORTRAN 77 program (see also [9]):

```
      SUBROUTINE MG (i, l, u^l, r^l, p, m, q)
      INTEGER p, q
      it(l) = i $ k = l
1     IF (k. EQ. 1) GOTO 4
2     CALL MOOTHING (r^k, u^k, p)
      r^(k-1) = RESTRICTION (r^k)
      k = k - 1 $ u^k = 0 $ it(k) = m
      GOTO 1
4     CALL DIRECTSOLVER (r^1, u^1)
5     If (k. EQ. l) RETURN
      k = k + 1
      δu^k = PROLONGATION (u^(k-1))
      r^k = r^k - A^k δu^k $ u^k = u^k + δu^k
      CALL SMOOTHING (r^k, u^k, q)
      it(k) = it(k) - 1
      IF(it(k). EQ. zero) GOTO 5
      GOTO 2
      END 'OF MG'
      SUBROUTINE SMOOTHING (r^k, u^k, pq)
      INTEGER pq
      DO 1 I = 1, pq
      δu^k = RELAXATION SCHEME (r^k)
      r^k = r^k - A^k δu^k $ u^k = u^k + δu^k
1     CONTINUE
      RETURN $ END 'OF SMOOTHING'
```

One call to subroutine MG $(i, l, u^l, r^l, p, m, q)$ performs i iterations of the basic multigrid cycle, where l is the number of levels, k $(= l,..., 1)$, u^l is the initial solution at level l (taken equal to zero in the present examples), and r^l is the corresponding residue at level l. The parameters p, q, and m specify the multigrid strategy, m being the number of times the coarse level correction is entered consecutively.

The only operators that remain to complete the description of this MG algorithm are the restriction, prolongation, and coarse level equations A^k.

Let a panel distribution on level l be denoted by h_i^l $(i = 1,..., n^l)$, where h is the panel length and n^l the number of panels. Define the coarse levels recursively by

$$n^{k-1} = \tfrac{1}{2}n^k \qquad \text{and} \qquad h_i^{k-1} = h_{2i-1}^k + h_{2i}^k \qquad (i = 1,..., n^{k-1}).$$

Let the restriction operator R_{ij}^k $(i = 1,..., n^{k-1} + n_c;\ j = 1,..., n^k + n_c)$ and the prolongation P_{ij}^k $(i = 1,..., n^k + n_c; j = 1,..., n^{k-1} + n_c)$ be defined by

$$R_{ij}^k = h_j^k / h_i^{k-1}, \quad \text{for} \quad j = 1,..., n^k \quad \text{with} \quad i = \text{IFIX}((j+1)/2), \tag{23a}$$

$$R_{ij}^k = 1, \quad \text{for} \quad j = n^k + 1,..., n^k + n_c \quad \text{with} \quad i = j - n^{k-1}, \tag{23b}$$

$$P_{ij}^k = 1, \quad \text{for} \quad i = 1,..., n^k \quad \text{with} \quad j = \text{IFIX}((i+1)/2), \tag{23c}$$

$$P_{ij}^k = 1, \quad \text{for} \quad i = n^k + 1,..., n^k + n_c \quad \text{with} \quad j = i - n^{k-1}, \tag{23d}$$

$$R_{ij}^k = P_{ij}^k = 0, \quad \text{for all other pairs of integers } (i, j). \tag{23e}$$

If we let the fine level equations be given by Eq. (11) and be denoted by A^l, then we may define the coarse level equations recursively by [10]

$$A^{k-1} = R^k A^k P^k, \tag{24}$$

which choice has been motivated by the results of Wesseling [11], who found the Galerkin coarse grid approximation (Eq. (24)) to be better than coarse grid discretization of the continuous problem.

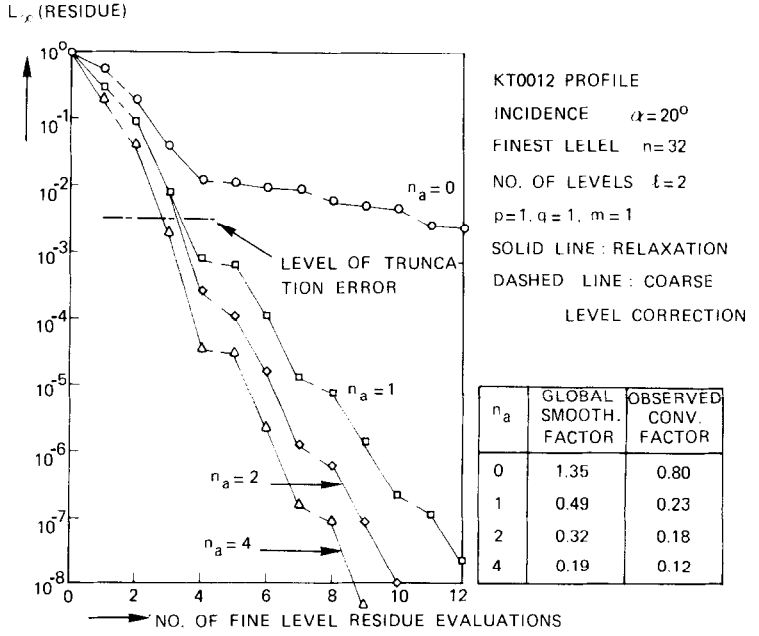

n_a	GLOBAL SMOOTH. FACTOR	OBSERVED CONV. FACTOR
0	1.35	0.80
1	0.49	0.23
2	0.32	0.18
4	0.19	0.12

FIG. 6. Convergence history of MG algorithm; 2 levels, source method, AF scheme.

Multigrid Convergence

In this section we illustrate the convergence characteristics of the MG algorithm described above by applying it to a number of potential flow problems, restricting ourselves to the source method and the AF scheme.

The first example pertains to the KT0012 profile, shown in Fig. 1, placed in a uniform flow and at an angle of attack of 20 degrees. The AF scheme used is characterized by the logical expression (22). The convergence history, the norm L_∞ of the residue as a function of the number of finc grid residue evaluations, is shown in Fig. 6, where we have chosen $n = 32$, $l = 2$, $p = 1$, $q = 1$, $m = 1$. Here we have defined

$$L_\infty(r^l) = \|r^l(v)\|_\infty / \|r^l(v=0)\|_\infty, \tag{25}$$

being the ratio of the maximum norm of the curent (v) residual vector r^l and the maximum norm of the initial ($v = 0$) residue, i.e., the right-hand side of Eq. (11). The observed convergence factor in Fig. 6 is about twice as good as the global smoothing factor which represents an upper bound of the convergence factor of the high frequencies obtained from a one-level analysis. These findings indicate that $\bar{\lambda}$ is a rather conservative estimate, although it is very realistic with respect to the effect of the nonzero pattern n_a.

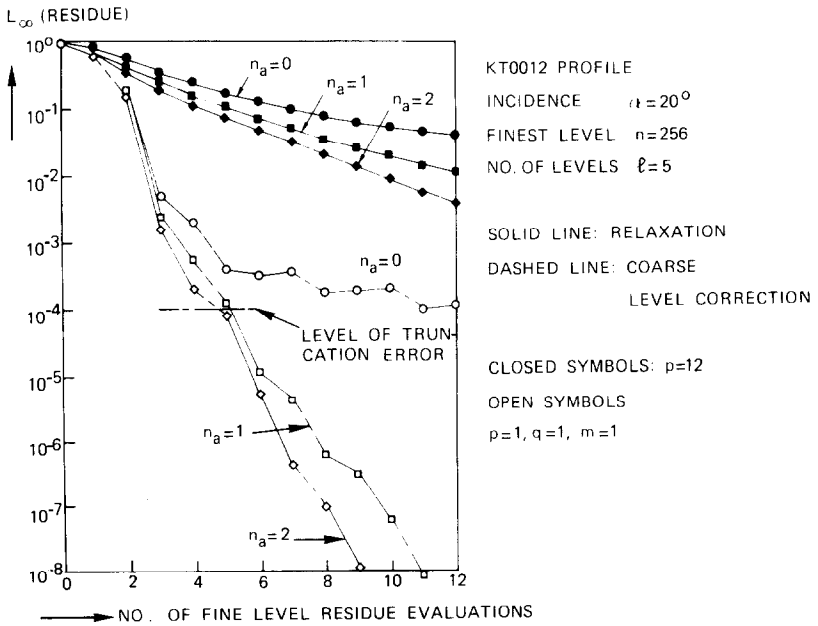

FIG. 7. Convergence history of MG algorithm; 5 levels, source method, AF scheme.

TABLE IV

Work Units per 10^{-1} Reduction[a] in the Residue over a Range of Strategies[b]

p	q	m	Work units per digit	p	q	m	Work units per digit
0	1	1	2.7	2	1	1	2.5
0	2	1	2.2	2	2	1	2.3
1	0	1	2.2				
1	1	1	2.2	0	1	2	4.3
1	2	1	2.2	0	1	2	4.3
1	2	1	2.2	1	0	2	5.3
2	0	1	2.0	1	1	2	3.6

[a] Average values over last 2 MG cycles of a total of 4 MG cycles.
[b] AF smoothing; $n_a = 1$; KT 0012, $\alpha = 20°$, $n = 245$, $l = 5$, $i = 4$.

Increasing the number of levels to 5 (see Fig. 7) does not change the asymptotic MG convergence rate, although the initial convergence improves somewhat. Using the AF scheme as a classical iteration procedure (Fig. 7), i.e, omitting the coarse level corrections, is found to be quite ineffective as should have been expected from the Fourier analysis.

Let us define the computational work associated with one residue evaluation at the finest level as one work unit in order to be able to compare various multigrid strategies. Results are given in Table IV, indicating costs ranging from 2.0 to 2.7 work units per 10^{-1} reduction in the maximum norm of the residual vector over a range of strategies p, q with $m = 1$. Convergence to the level of the truncation error is obtained within 2 MG cycles. Multigrid strategies with $m = 2$, i.e., entering the coarse level correction two times consecutively, are found to be computationally less efficient, see Table IV.

The second example illustrates the convergence of the MG algorithm when applied to the problem of a wing plus flap configuration shown in Fig. 8. The convergence history is shown in Fig. 9. It is observed that the AF smoothing is quite effective for $n_a \geqslant 1$, although we have just repeated the nonzero pattern for single-component airfoils to the wing alone and flap alone for $(i, j) \leqslant n$. No zero entries for $i > n$ or $j > n$ have been created. This zero pattern, which neglects all connections in the matrix between wing and flap for $(i, j) \leqslant n$, results in acceptable AF smoothing for a gap of 2.6 percent. In the limit of vanishing gap size for a fixed paneling, however, we would, of course, have to take some nonzero entries representing the flap/wing connections into account if acceptable AF smoothing is to be retained in this limit; this has been confirmed by numerical experiments. These observations clearly lead to the requirement that all near field connections have to be taken into account during the construction of a particular AF smoothing scheme.

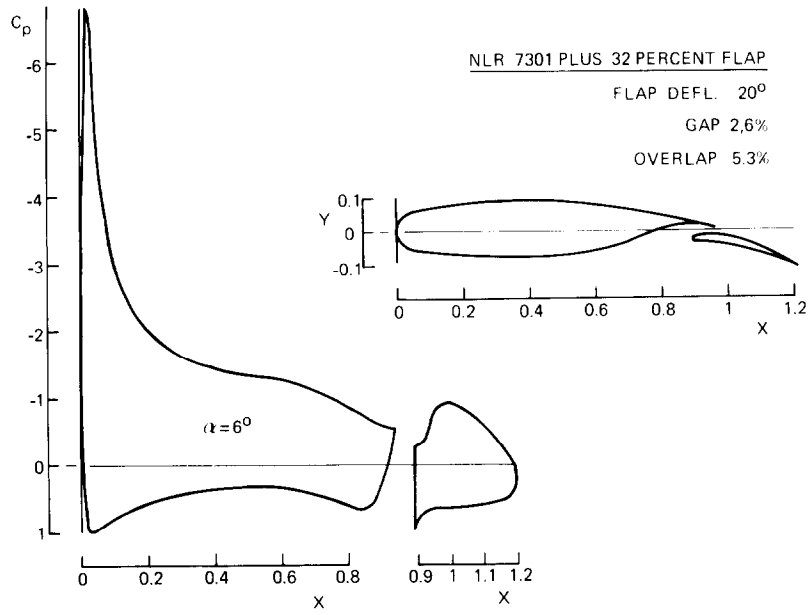

FIG. 8. Pressure distribution of NLR 7301 plus 32 percent flap at 6 degrees incidence.

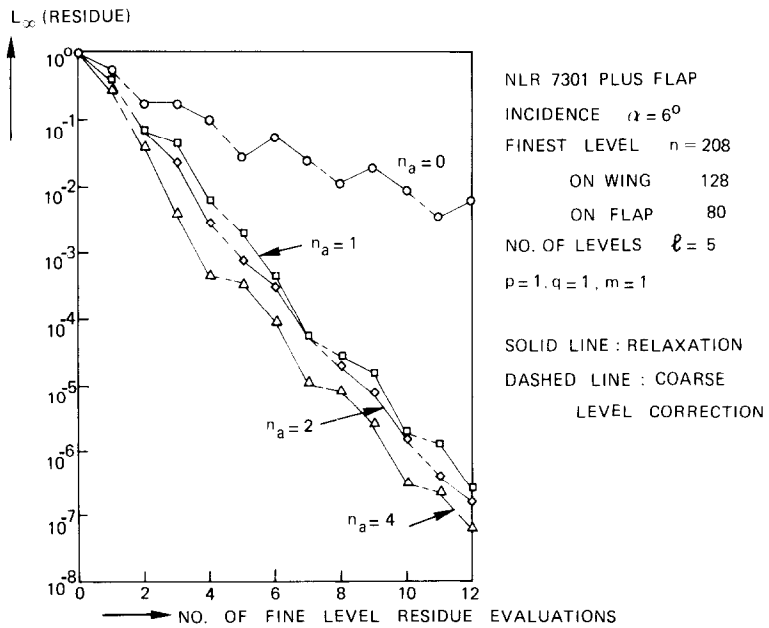

FIG. 9. Convergence history of MG algorithm; 5 levels, source method, AF scheme.

Conclusion

Approximate factorization (AF) relaxation schemes provide a smoothing capability that allows one to construct a fast multigrid method for solving integral equations of the second as well as of the first kind.

The local mode analysis of Brandt [4] is applied for the special cases of an unbounded flat plate and circular cylinder and predicts the qualitative difference between multigrid problems of the first and second kind, where the former has a smoothing factor independent of h and the latter a smoothing factor proportional to h. For more realistic geometries having surface slope discontinuities such as airfoils, Fourier analysis predicts no qualitative difference between smoothing factors obtained with the AF scheme when applied to integral equations of either the first or second kind.

Numerical experiments show that convergence to the level of the truncation error of a second-order accurate integral method can be obtained within two MG cycles.

Appendix

Let a residual correction iterative scheme to solve the matrix equation, $Au = f$, be given by

$$\delta u^{(\nu+1)} = \tilde{A} r^{(\nu)}, \tag{A1}$$

$$u^{(\nu+1)} = u^{(\nu)} + \delta u^{(\nu+1)}, \tag{A2}$$

$$r^{(\nu+1)} = r^{(\nu)} - A\,\delta u^{(\nu+1)}, \tag{A3}$$

with the iteration index ν (= 0, 1, 2,...). Setting the initial solution $u^{(0)}$ equal to zero results in an initial residue $r^{(0)}$ equal to the right-hand side f. The column vector $\delta u^{(\nu+1)}$ is the correction to the approximate solution $u^{(\nu)}$ and $\tilde{A}$ is an approximate inverse of A. This inverse is either constructed (NRS scheme) or implied by the AF scheme. For the latter case we have $\tilde{A} = (LU)^{-1}$.

This iterative scheme results in an error amplification matrix M_e defined by

$$u^{(\nu+1)} - u = M_e(u^{(\nu)} - u), \qquad \nu = 0, 1, 2,..., \tag{A4}$$

which reads $M_e = I - \tilde{A}A$. The corresponding residue amplification matrix, defined by

$$r^{(\nu+1)} = M_r r^{(\nu)}, \qquad \nu = 0, 1, 2,..., \tag{A5}$$

is equal to $M_r = I - A\tilde{A}$. In case A and $\tilde{A}$ are either circulant matrices or infinite Toeplitz matrices, one finds $\tilde{A}A = A\tilde{A}$ and $M_e = M_r$. For a more general matrix A resulting from the airfoil problem of Eq. (11), we have chosen to analyze the residue amplification matrix M_r. The choice of the zero pattern (22) in the AF scheme when applied to the $(n + n_c)$-dimensional matrix equation (11) results in an n-dimensional matric $M_r = I - A\tilde{A}$.

REFERENCES

1. W. HACKBUSCH, "Die schnelle Auflösung der Fredholmschen Integralgleichung zweiter Art," Report 78-4, Universität zu Köln, Cologne, 1978.
2. H. SCHIPPERS, "The Automatic Solution of Fredholm Equations of the Second Kind," Report NW 99/80, Mathematisch Centrum, Amsterdam, 1980.
3. J. W. SLOOFF, "Requirements and Developments Shaping a Next Generation of Integral Methods," paper presented at IMA Conference on Numerical Methods in Aeronautical Fluid Dynamics, University of Reading, England, 1981.
4. A. BRANDT, *Math. Comput.* **31** (138) (1977), 333.
5. J. L. HESS, *Comput. Metholds Appl. Mech Eng.* **5** (1975), 11.
6. F. T. JOHNSON AND P. E. RUBBERT, "Advanced Panel-Type Influence Coefficient Methods Applied to Subsonic Flows," AIAA Paper No. 75-50, 1975.
7. J. L. HESS, "Consistent Velocity and Potential Expansions for Higher-Order Surface Singularity Methods," Report MDCJ 6911, McDonnell Douglas Corp., Long Beach, CA, 1975.
8. J. A. MEIJERINK AND H. A. VAN DER VORST, *Math. Comput.* **31** (137) (1977), 148.
9. W. HACKBUSH, "Introduction to Multigrid Methods for the Numerical Solution of Boundary Value Problems," Von Karman Institute for Fluid Dynamics, Lecture Series 1981-5, 1981.
10. P. O. FREDERICKSON, "Fast Approximate Inversion of Large Sparse Linear Systems," Mathematics Report 7-75, Lakehead Univ., Thunder Bay, Ontario, Canada, 1975.
11. P. WESSELING, "Theoretical and Practical Aspects of a Multigrid Method," Department of Math. Report NA-37, Delft University of Technology, The Netherlands, 1980.